New Approaches to Multifrequency Sp Stacking Tested in the Anatolian Region

J. Hua[1] (junlin_hua@brown.edu), K. M. Fischer[1], M. Wu[1] and N. Blom[2]

[1] Department of Earth, Environmental and Planetary Sciences, Brown University, Providence, RI 02906, USA.

[2] Bullard Laboratories, Department of Earth Sciences, University of Cambridge, Madingley Rise, Cambridge CB3 0EZ, UK.

Contents of this file

Figures S1 to S9

Introduction

This file contains the supplementary figures for the article. Methods used to generate these figures and their interpretation are discussed in the main text.
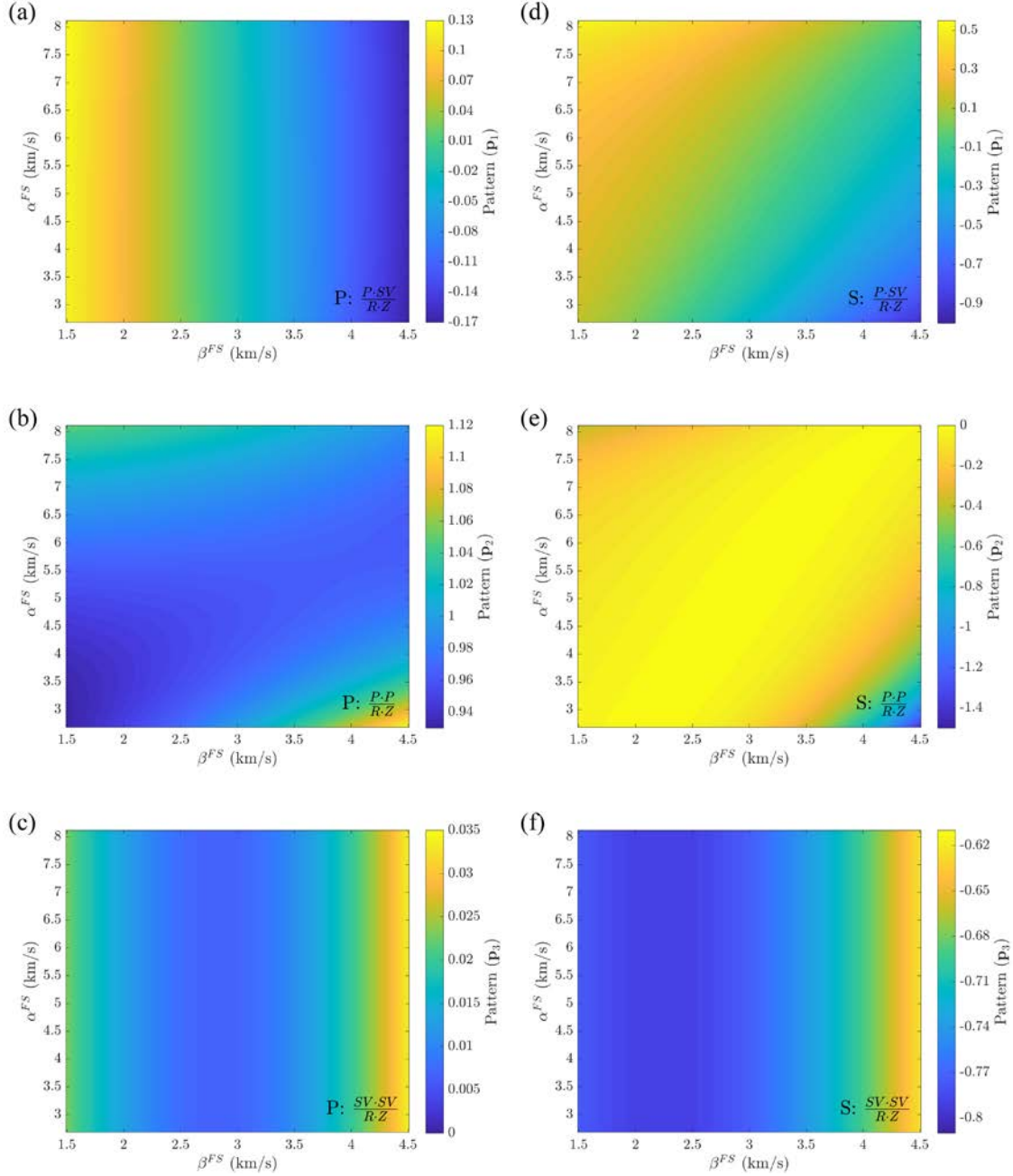
Figure S1. (a)-(c) Particle motion patterns similar to Figures 3a to 3c, but for the real P arrival used in Figure 4. (d)-(f) Particle motion patterns similar to Figures 3e to 3g, but for the real S arrival used in Figure 3. Colors show the value of the pattern for varying α^{FS} and β^{FS}; (a) $\mathbf{C}_1$ pattern; (b) $\mathbf{C}_2$ pattern, (c) $\mathbf{C}_3$ pattern for P arrivals; (d) $\mathbf{C}_1$ pattern; (e) $\mathbf{C}_2$ pattern, (f) $\mathbf{C}_3$ pattern for S arrivals. The label in the bottom right corner indicates the arrival phase and the equation for the pattern.
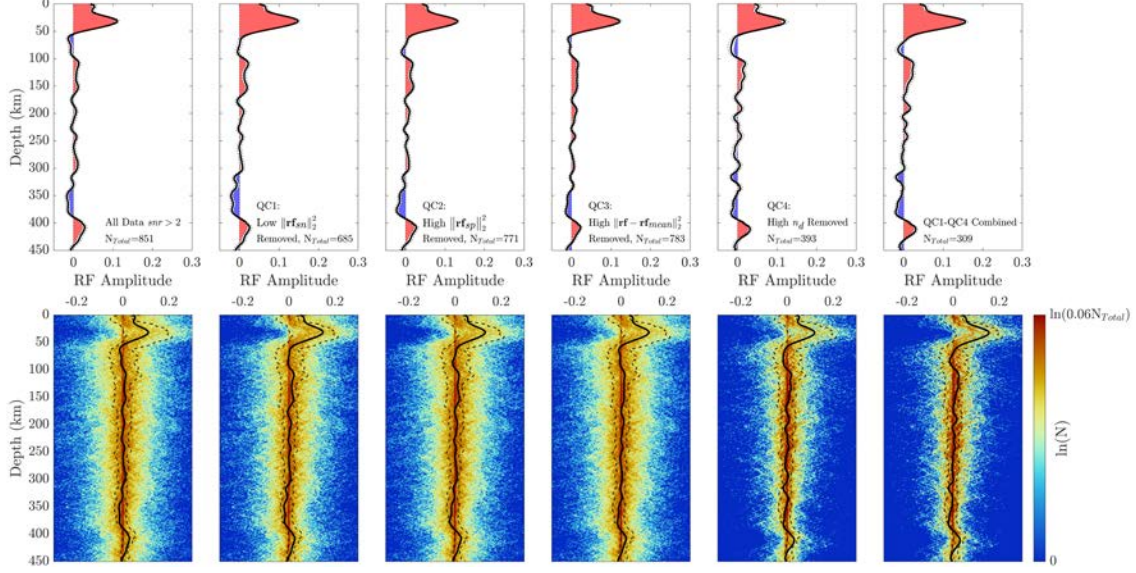
Figure S2. Effects of data quality criteria (QC) on receiver functions from the station ANTO (IU network) located at 39.87°N, 32.79°E. Sp receiver function amplitudes have their signs flipped in this figure to match the Ps convention. The first row shows stacked receiver function amplitudes migrated with the 1D velocity model at the station from Blom et al. (2020). The black solid line shows the stacked receiver function amplitude, while the dashed lines indicate one standard deviation uncertainties. Standard deviations are calculated based on eq. (26) while weighting all receiver functions equally. Red phases represent positive velocity gradients and blue phases represent negative velocity gradients. The second row shows the natural logarithm of the number of receiver functions that lie within a given depth-amplitude pixel, so these plots illustrate the distribution of individual receiver functions. Black solid lines show the stacked receiver function amplitude as in the first row, and black dashed lines show $\mathbf{rf}_{min}$ and $\mathbf{rf}_{max}$ obtained from the synthetic seismograms with the Blom et al. (2020) model. Panels in this row have a different amplitude scale on their horizontal axes than those in the first row, and the color bar is from 0 (one or no waveform) to $\ln(0.06 N_{Total})$. N_{Total} is the number of receiver functions that pass the quality control and are used for the stack, and its value is labelled in the first row. The six columns illustrate the effects of different data quality criteria. The first column is based on all data that satisfy the signal-to-noise ratio higher than 2 requirement, while other columns also satisfy this requirement in addition to the labelled criteria. The second column has receiver functions with small $\left\|\mathbf{rf}_{sn}\right\|_2^2$ removed; the third column has ones with large $\left\|\mathbf{rf}_{sp}\right\|_2^2$ removed; the fourth column has ones with large $\left\|\mathbf{rf} - \mathbf{rf}_{mean}\right\|_2^2$ removed; the fifth column has ones with large n_d removed; and the sixth column shows the combined effect of all quality controls from column 2 to 5. Panels in the first row are labelled by the quality criterion and the number of receiver functions that pass (bottom right corner). The quality criteria are described in Section 3.
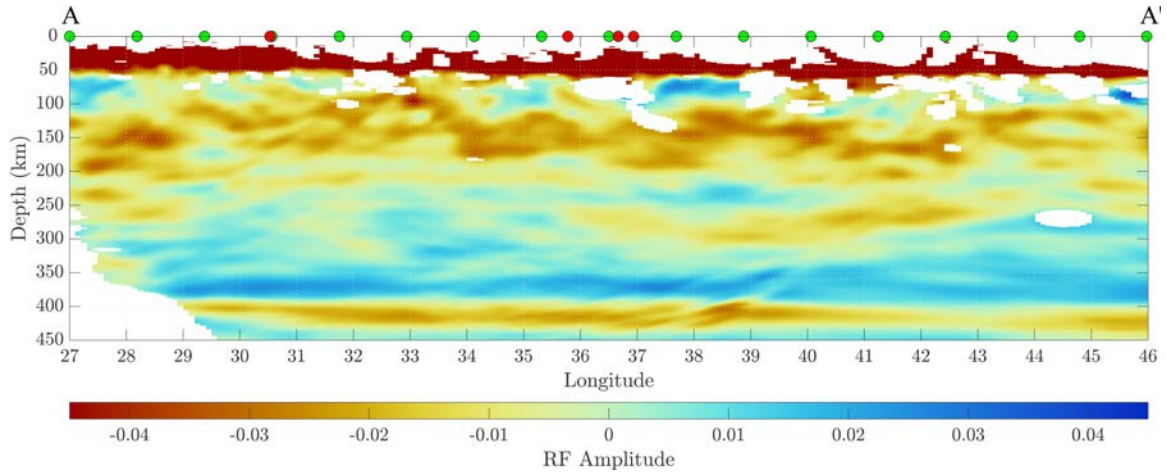
Figure S3. Sp CCP stack amplitudes on profile A-A', with symbols and notations the same as in Figure 11a. The stack is obtained with all receiver functions that pass the two Moho related quality controls which remove data with small $\left\| \mathbf{rf}_{sn} \right\|_2^2$ or large $\left\| \mathbf{rf}_{sp} \right\|_2^2$, as described in Section 3. With only the Moho criteria, we retain 45,872 receiver functions, approximately twice the number as in the final version of the stack which is shown in Figure 11a. Both versions of the stack (Figure 11a versus this figure) contain the same overall features. However, the negative phase at 80-150 km is less coherent here, illustrating the usefulness of the additional quality criteria employed in Figure 11a.
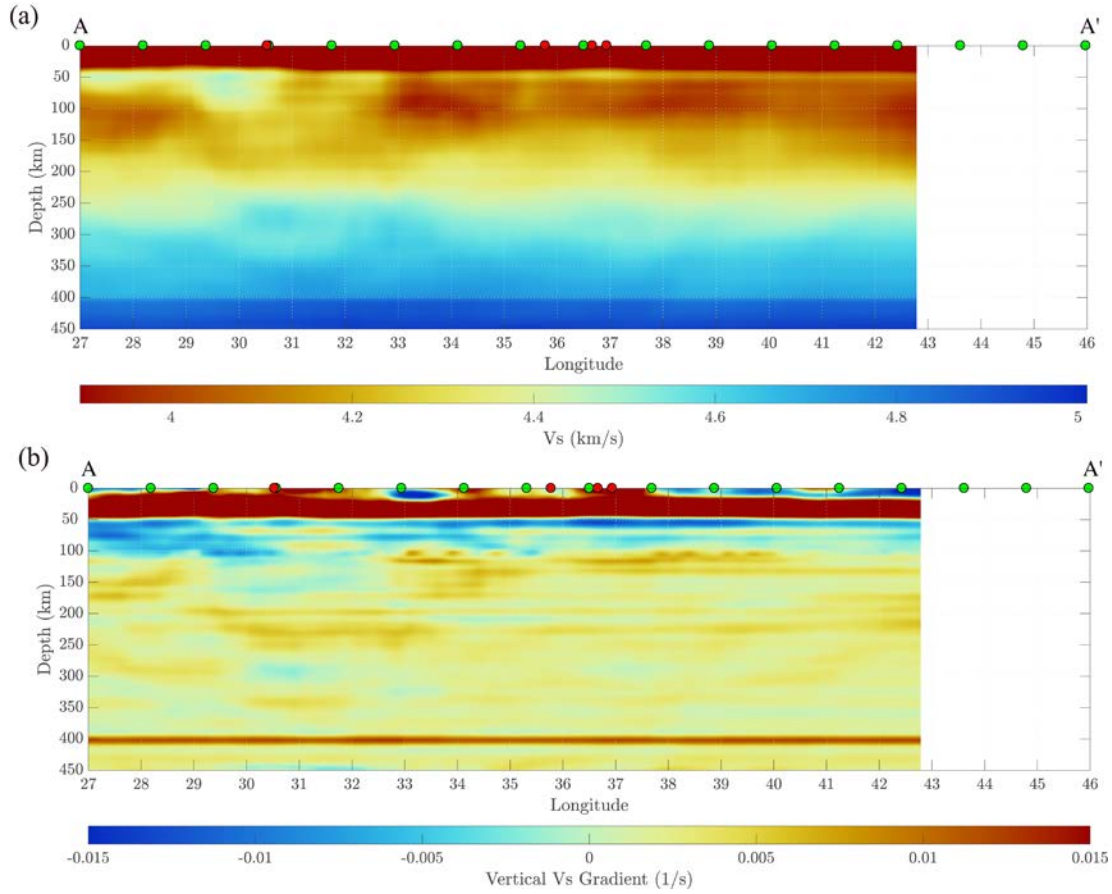
Figure S4. Shear velocity model on profile A-A'. (a) Shear wave velocity from Fichtner et al. (2013). Velocities exceeding the limit of the color bar are shown by the color at the limit (e.g. crustal velocity). (b) Vertical shear wave velocity gradient from Fichtner et al. (2013) smoothed over a 5 km depth window. The velocity model is consistent with the negative Sp phase at depths of 80 – 150 km, in the sense that the velocity model contains a low velocity layer above 150 km depth and positive velocity gradients from 33°E to 40°E at 100 – 130 km depths, but no clear gradients east of 40°E. However, the strong positive velocity gradient at 230 km depth from 29°E to 33°E in the velocity model does not correspond to a feature in the Sp CCP stack.
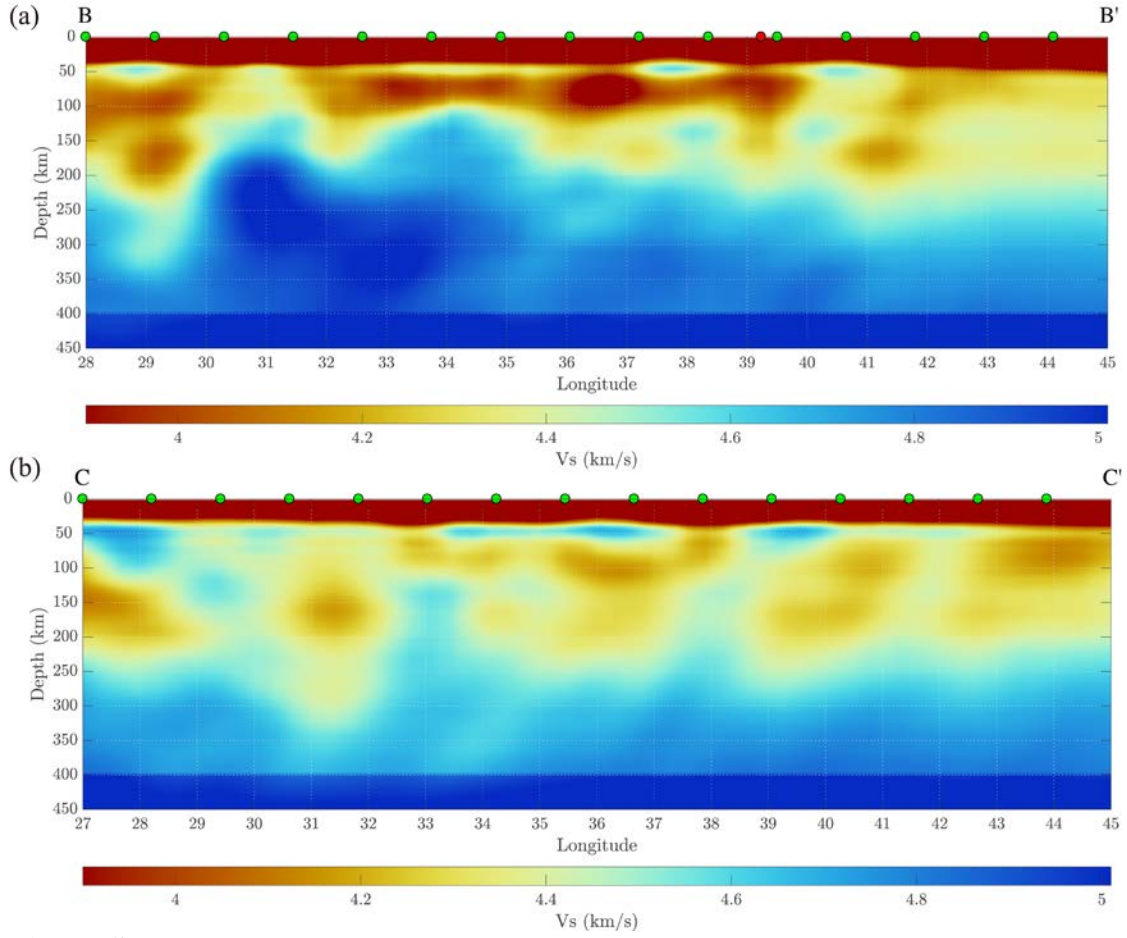
Figure S5. Shear velocity model on east-west profiles B-B' and C-C' from Blom et al. (2020). Similar to Figure 13a. Velocities exceeding the limit of the color bar are shown by the color at the limit (e.g. crustal velocities). The low velocity layer at 50-110 km depth in (a) broadly agrees with the observed positive velocity gradient in Figure 14a. The absence of a strong low velocity anomaly in (b) agrees with the lack of negative Sp phases in Figure 14b.
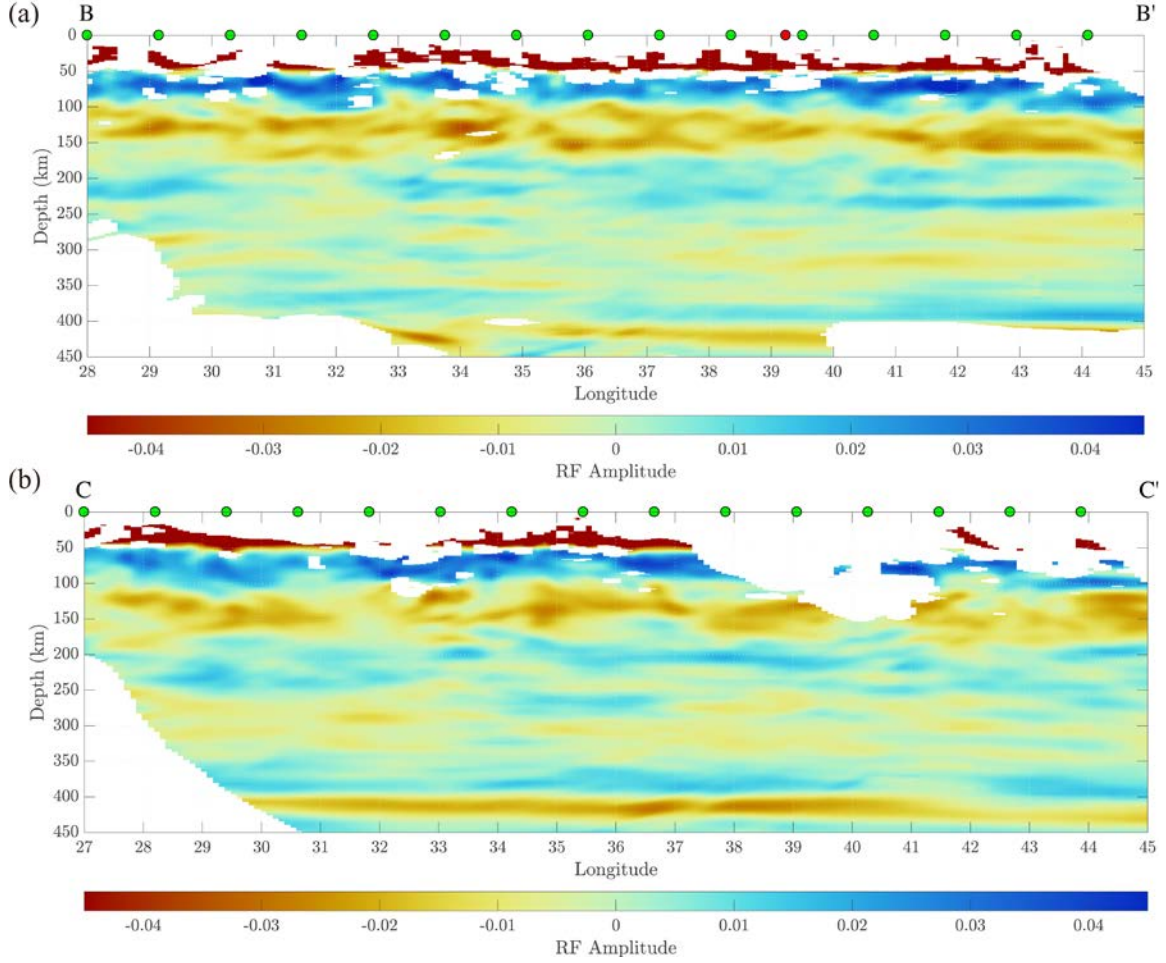
Figure S6. Sp CCP stack amplitudes on east-west profiles B-B' and C-C'. Similar to Figure 14, but using the 2-20 s bandpass filter before deconvolution which is also used in Figure 16a. Symbols and notations identical to Figure 11a. Profile locations shown in Figure 1.
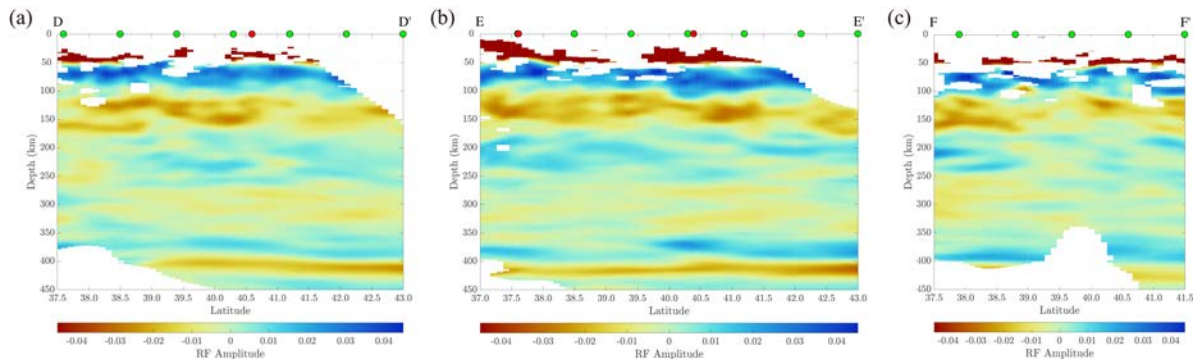

Figure S7. Sp CCP stack amplitudes on north-south oriented profiles D-D', E-E' and F-F'. Similar to Figure 15, but using a 2-20 s bandpass filter before deconvolution. Symbols and notations identical to Figure 11a, but horizontal axes are labeled with latitude. Profile locations shown in Figure 1.
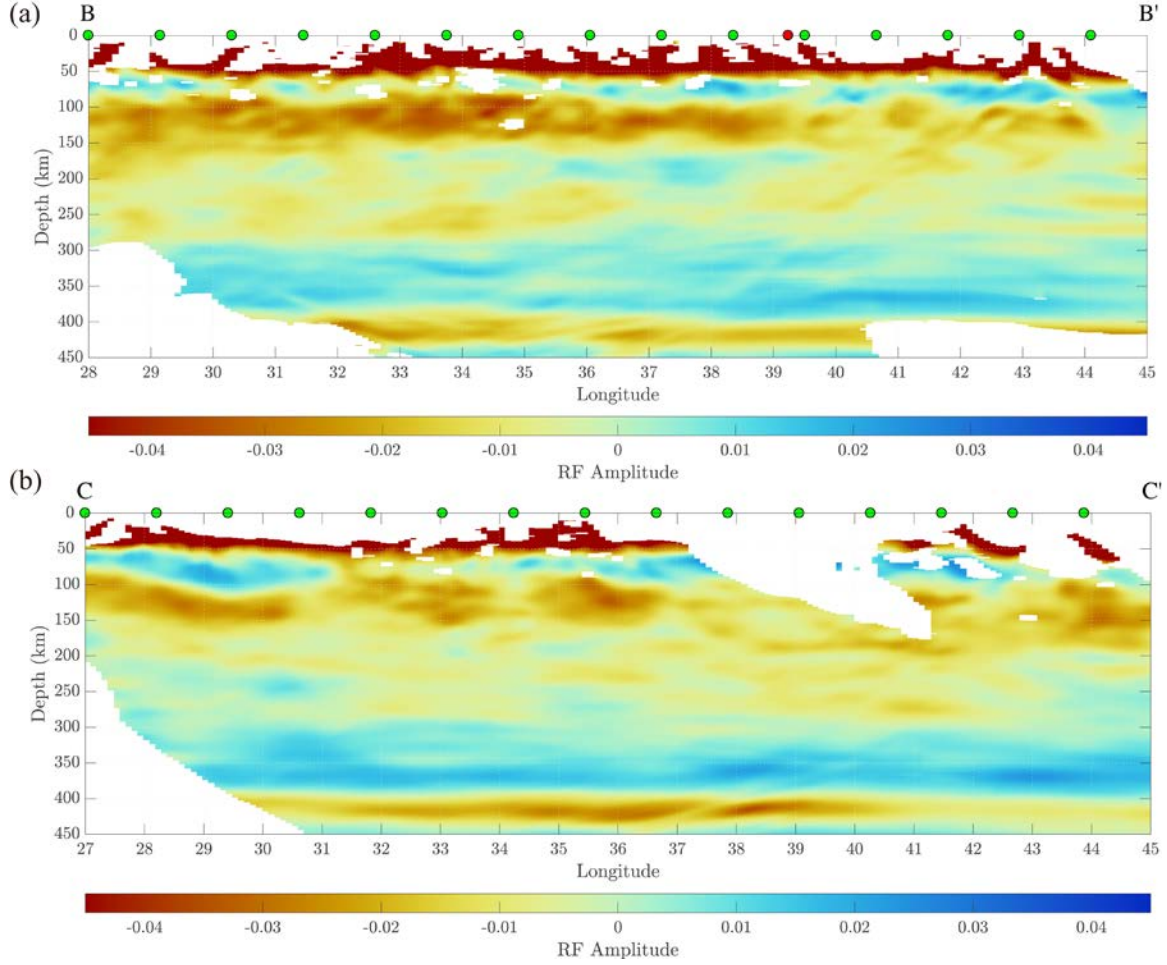
Figure S8. Sp CCP stack amplitudes on east-west profiles B-B' and C-C'. Similar to Figure 14, but using the 10-100 s bandpass filter before deconvolution which is also used in Figure 16b. Symbols and notations identical to Figure 11a. Profile locations shown in Figure 1.
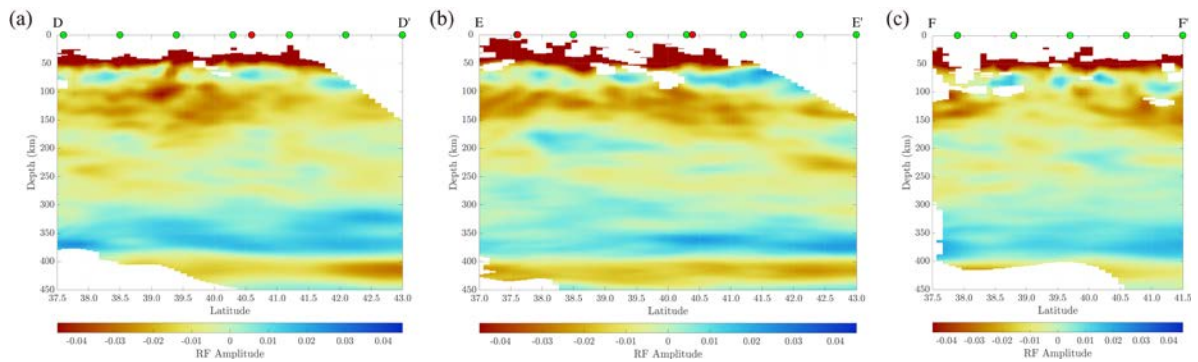

Figure S9. Sp CCP stack amplitudes on north-south oriented profiles D-D', E-E' and F-F'. Similar to Figure 15, but using a 10-100 s bandpass filter before deconvolution. Symbols and notations identical to Figure 11a, but horizontal axes are labeled with latitude. Profile locations shown in Figure 1.